Multi-Layer ToF: Comparison of different multipath resolve methods for indirect 3D time-of-flight

1st Jonas Gutknecht
Institute of Signal Processing and Wireless Communications
ZHAW Zurich University of Applied Sciences
Winterthur, Switzerland
jonas.gutknecht@zhaw.ch

2nd Teddy Loeliger
Institute of Signal Processing and Wireless Communications
ZHAW Zurich University of Applied Sciences
Winterthur, Switzerland
teddy.loeliger@zhaw.ch

***Abstract*—Multipath Interferences (MPI) represent a significant source of error for many 3D indirect time-of-flight (iToF) applications. Several approaches for separating the individual signal paths in case of MPI are described in literature. However, a direct comparison of these approaches is not possible due to the different parameters used in these measurements. In this article, three approaches for MPI separation are compared using the same measurement and simulation data. Besides the known procedures based on the Prony method and the Orthogonal Matching Pursuit (OMP) algorithm, the Particle Swarm Optimization (PSO) algorithm is applied to this problem. For real measurement data, the OMP algorithm has achieved the most reliable results and reduced the mean absolute distance error up to 96% for the tested measurement setups. However, the OMP algorithm limits the minimal distance between two objects with the setup used to approximately 2.7 m. This limitation cannot be significantly reduced even with a considerably higher modulation bandwidth.**

***Index Terms*—indirect time-of-flight, multi path interference, Prony method, orthogonal matching pursuit, particle swarm optimization**

I. Introduction

The 3D iToF measurement method using Continuous Wave (CW) modulation is an established technique found in many fields of application. A 3D iToF camera consists of an illumination and a photosensitive sensor element plus corresponding evaluation circuity. This measurement method is shown in simplified form in Fig. 1. The illumination sends an optical, CW modulated Tx signal with modulation frequency f_n, which then is reflected by the objects in the Field of View (FoV) of the camera. This reflected Rx signal is captured by the sensor element and demodulated using a homodyne receiver structure. For each pixel, the phase φ_n and amplitude a_n of the demodulated signal m_n, described in (1), is measured. For the case of a single reflection $K = 1$, with known f_n and speed of light c, the object distance d_0 can thus be estimated according to (2).

$$m_n = \sum_{k=0}^{K-1} a_k e^{\frac{4j\pi f_n d_k}{c}} = a_n e^{\varphi_n} \tag{1}$$

$$d_0 = \frac{c\varphi_n}{4\pi f_n} \qquad , K = 1 \tag{2}$$

This method works well for many applications. However, there are scenes, where the assumption of only one reflexion per pixel does not match the reality. Several reflexions can be caused e.g. by semi-transparent objects, corners, or due to straylight. In this case $K > 1$ signals with the same frequency f_n but different phase φ_k and amplitude a_k are superimposed and thus the resulting phase φ_n and amplitude a_n do not correspond to a real path. This error is known as MPI and is visible in the point cloud in Fig. 1 along the contour of the person.

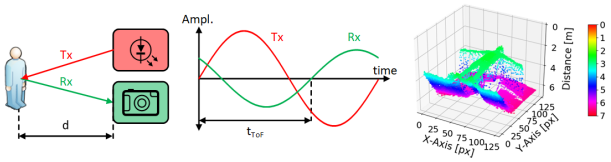

Fig. 1. 3D iToF camera principle

There are different approaches to resolve K signal paths using N iToF measurements with different modulation frequencies [1], [2]. In [3] spectral estimation for $K = 2$ and $N = 5$ is described based on the Prony method and tested on simulation data with modulation frequencies in the range of 22 MHz to 66 MHz. The general case with arbitrary K and at least $N = 2K + 1$ is described in [4]. In both works the spectrum estimation is a closed form solution based on Prony. With a measurement using $N = 21$ frequencies in the range 52 MHz to 72 MHz, up to $K = 2$ signal paths were separated. In [5] the spectrum is estimated with the iterative greedy algorithm OMP for a general case with K signal paths. The method is tested with measurements using $N = 77$ frequencies in the range 0.07937 MHz to 61.1149 MHz and resolved for the case $K = 3$.

Each of these methods could reduce the error due to MPI dramatically. However, a comparison is quite difficult due to the different measurement settings. The aim of this work is to compare three different methods for MPI separation using the same data. In addition to the known approaches based on Prony and OMP, the PSO algorithm, which exhibits a certain robustness with respect to local minima due to the stochastic component, is applied to MPI separation. To the best of our knowledge, the PSO method has not been used for this application so far. Furthermore, the minimum separable

distance difference between two objects is being investigated.

In section II the MPI separation measurement procedure and the three methods are briefly described. Subsequently, the results of the methods are presented in section III and discussed in section IV. Section V concludes this work.

II. MPI Separation

As a data basis for MPI separation, the test scene in the FoV is measured with $N = 14$ equally distributed modulation frequencies in the range from $f_0 = 10.0$ MHz to $f_{N-1} = 36.0$ MHz. This results in a complex vector $\boldsymbol{m}$ per pixel of length N with elements described in (1). A DME 660 from ESPROS Photonics Corporation was used for these measurements, and the amplitude and phase response of the camera have been calibrated. In addition to the measured data, synthetic data from simulations have also been used. The MPI separation methods search for a maximum of $K_R = 3$ signal paths. The three methods are briefly described below. Detailed descriptions of the Prony and OMP methods are provided in [2]–[5].

A. Prony Method

According to theory, the Prony method can exactly separate K signal paths with $N > 2K + 1$ modulation frequencies [4]. Since this method is not an iterative procedure but a closed form method, the computational effort is low. To reduce the sensitivity to measurement errors, the data are pre-processed with the Cadzow denoising procedure as suggested in [3], using at most five iteration steps and a final rank of $K_R = 3$.

B. Orthogonal Matching Pursuit

The separation with the OMP algorithm according to [5] is based on a dictionary $\boldsymbol{\Psi}$ with entries $\boldsymbol{\psi}_\ell$, which corresponds to the normalised theoretical measurement vector $\boldsymbol{m}$ for the given modulation frequencies and a discrete distance $\widetilde{d}_\ell$. In the context of this work, a dictionary with $L = 200$ entries and $\widetilde{d}_\ell \in [0, 10]$ m was used. The OMP algorithm approximates in iteration step i the measurement vector $\boldsymbol{m}$ with the linear combination $\widetilde{\boldsymbol{m}}_i$ of a subset of $\boldsymbol{\Psi}$. This subset is extended in each iteration step by the single entry $\boldsymbol{\psi}_\ell$ which has the highest correlation with the current residual $\boldsymbol{m} - \widetilde{\boldsymbol{m}}_i$.

C. Particle Swarm Optimization

With the PSO algorithm, the solution space is searched with $S = 50$ particles, during $I = 30$ iteration steps for a global minimum of the objective function $f_{obj}(\widetilde{\boldsymbol{m}})$. The solution space is spanned by $K_R = 3$ amplitude and distance estimates.

$$\widetilde{m}_n = \sum_{k=0}^{K_R-1} \widetilde{a}_k e^{\frac{4j\pi f_n \widetilde{d}_k}{c}} \tag{3}$$

$$f_{obj}(\widetilde{\boldsymbol{m}}) = \|\widetilde{\boldsymbol{m}} - \boldsymbol{m}\|_2 \tag{4}$$

The behaviour of the particles is modelled on the swarm behaviour known from nature and is controlled by particles inertia weight $\omega = 0.8$, weight of particles optimum $\eta_1 = 0.8$ and weight of swarm optimum $\eta_2 = 0.8$. For this work, the PSO implementation of [6] is used.

III. Performance Comparison

A benchmark measurement was used to compare the three methods against each other. The setup consists of a wire grid at a distance of $d_0 = 2.4$ m with a wire diameter of 2 mm and a mesh size of approx. 1.0×1.0 cm in front of a white wall at a distance of $d_1 = 8.0$ m. Since the mesh size of the grid is smaller than the pixel size in d_0, two reflections are mapped onto each pixel and thus cause MPI as shown in Fig. 2a. The measurement data at f_0 and the results of the MPI separation based on the Prony, OMP and PSO method are shown in Fig. 2 and Fig. 3 as 3D point cloud and distance histogram, respectively. Whereas the standard measurement delivers completely wrong distances between 5.0 and 7.5 m, the three methods investigated can clearly separate the two layers at 2.4 and 8.0 m. In Table I the mean value μ_e and standard deviation σ_e of the absolute distance errors are presented. A 58×74 pixel image area was used for this evaluation. Using simulated data, the minimum separable distance difference $\Delta d_{min} = |d_0 - d_1|$ of two objects with similar amplitude $a_0 = a_1$ was also investigated, neglecting stochastic and systematic measurement errors. These values can also be seen in Table I and could be confirmed with real measurements.

TABLE I
Distance error statistics of benchmark measurement

Dataset	μ_e	σ_e	Δd_{min}
standard measurement with f_0	1.75 m	0.64 m	
Prony	0.10 m	0.07 m	$>$ 0.00 m
OMP	0.07 m	0.04 m	$\approx$ 2.70 m
PSO	0.16 m	0.14 m	$\approx$ 1.50 m

IV. Discussion

A. Distance Error

For all tested methods the distance error caused by MPI can be significantly reduced and the individual signal paths separated. In the ideal case without measurement errors, the Prony method can be used to precisely separate the individual signal paths with little computational effort. However, measurement errors in the data can lead to considerable distance errors despite pre-processing with Cadzow denoising. In contrast, the OMP method provides the most reliable data for all real benchmark measurements performed. The noise in the absolute distance error of 0.04 m is below the distance resolution $\widetilde{d}_\ell - \widetilde{d}_{\ell+1} = 0.05$ m of the dictionary $\boldsymbol{\Psi}$. The PSO method has a high distance noise due to the stochastic component of the algorithm, which can be seen in Table I and Fig. 3d. Furthermore, the PSO method requires the highest computational effort of the tested methods.

B. Distance Difference

Due to the closed form of the Prony method, arbitrarily small distance differences can be separated in theory. In contrast, Δd_{min} for the PSO and OMP is limited by the used frequency range. For the PSO method, Δd_{min} is also limited

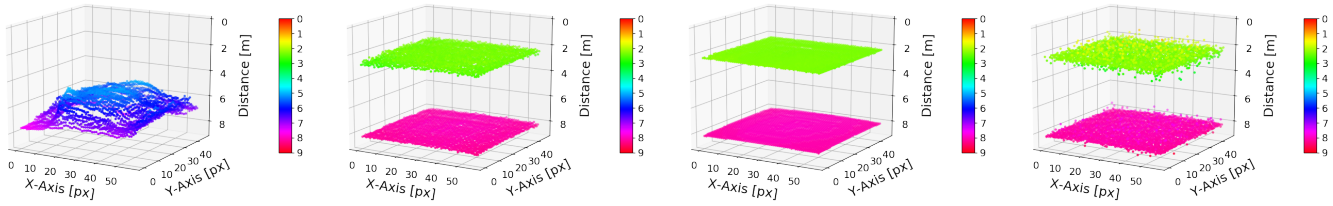

(a) measurement at $f_0 = 10$ MHz (b) MPI separation with Prony (c) MPI separation with OMP (d) MPI separation with PSO

Fig. 2. 3D point cloud of benchmark measurement

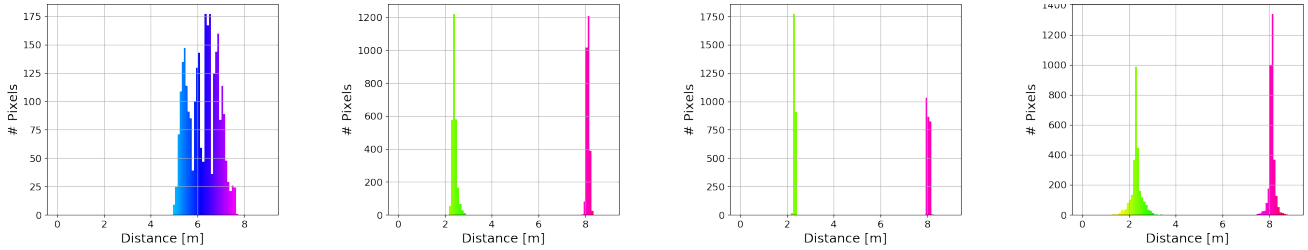

(a) measurement at $f_0 = 10$ MHz (b) MPI separation with Prony (c) MPI separation with OMP (d) MPI separation with PSO

Fig. 3. distance histogram of benchmark measurement

by the distance noise and is about 1.5 m in the setup used. For the OMP method, Δd_{min} is also limited by the selection of the dictionary entries $\boldsymbol{\psi}_\ell$ based on the correlation maximum between error vector and dictionary. At the first iteration step, the error vector corresponds to the measurement vector $\boldsymbol{m}$ and thus the real-valued part of the correlation function to $p(\widetilde{d}_\ell)$ according to (5).

$$p\left(\widetilde{d}_\ell\right) = \Re\left(\int_{f_0}^{f_N-1} e^{-j\frac{4\pi f \widetilde{d}_\ell}{c}} \sum_{k=0}^{K-1} a_k e^{\frac{4j\pi f d_k}{c}} df\right) = \sum_{k=0}^{K-1} a_k c\left(\widetilde{d}_\ell - d_k\right) \tag{5}$$

$$c\left(x\right) := \frac{c}{4\pi x}\left(\sin\left(\frac{4\pi f_{N-1} x}{c}\right) - \sin\left(\frac{4\pi f_0 x}{c}\right)\right) \tag{6}$$

The function $p(\widetilde{d}_\ell)$ for $K = 2$, $\Delta d = |d_0 - d_1|$ and $a_0 = a_1$ consists of the superposition of two sinc-like functions $c\left(x\right)$ shifted in x direction by d_0 and d_1 respectively. For small Δd, the function $p(\widetilde{d}_\ell)$ has a global maximum at $\frac{d_0+d_1}{2}$ and the paths are thus not properly separated. Separation is theoretically only possible from Δd_{min}, where this represents the minimum Δd for which the second derivative of the function $p(\widetilde{d}_\ell)$ exceeds 0 at the point $\frac{d_0+d_1}{2}$. This limitation is shown in Fig. 4 for different f_0 and modulation bandwidths $f_{N-1} - f_0$. Note that Δd_{min} does not fall below 0.5 m even for $f_n \in [50, 150]$ MHz.

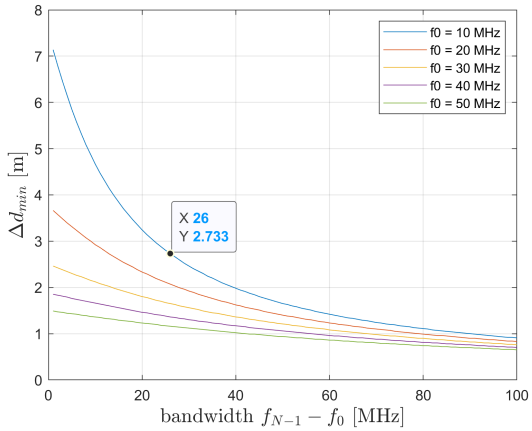

Fig. 4. Δd limitation for OMP method

V. Conclusion

MPI can be reliably resolved with the investigated methods and distance errors can be reduced by factors of 10 or more, depending on the scene. The OMP algorithm achieves the most reliable results even in case of error-prone measurements. However, the OMP algorithm considerably limits the minimum separable distance difference between the signal paths. For minor errors, the Prony method can be used to accurately separate the signal paths with low computational effort. With less restricted computational requirements, the PSO method with suitable optimisation of the parameters could be an adequate method for separating erroneous measurement data with small distance differences between the objects.

Acknowledgment

These research results were developed in collaboration with ESPROS Photonics Corporation. In particular, we would like to thank Beat De Coi, Udo Graf and Silvio Honegger for their excellent support and collaboration.

REFERENCES

[1] R. Whyte, L. Streeter, M. J. Cree and A. A. Dorrington, "Review of methods for resolving multi-path interference in Time-of-Flight range cameras," in Proc. IEEE Sensors, Valencia, Spain, Nov. 2014, pp. 629–632.

[2] M. Feigin, A. Bhandari, S. Izadi, C. Rhemann, M. Schmidt and R. Raskar, "Resolving Multipath Interference in Kinect: An Inverse Problem Approach," in IEEE Sensors Journal, May 2016, pp. 3419-3427.

[3] A. Kirmani, A. Benedetti and P. A. Chou, "SPUMIC: Simultaneous phase unwrapping and multipath interference cancellation in time-of-flight cameras using spectral methods", in Proc. IEEE ICME, Jul. 2013, pp. 1-6.

[4] A. Bhandari, M. Feigin, S. Izadi, C. Rhemann, M. Schmidt and R. Raskar, "Resolving multipath interference in Kinect: An inverse problem Approach," in Proc. IEEE Sensors, Valencia, Spain, Nov. 2014, pp. 614-617.

[5] A. Bhandari, A. Kadambi, R. Whyte, C. Barsi, M. Feigin, A. Dorrington, and R. Raskar, "Resolving multipath interference in time-of-flight imaging via modulation frequency diversity and sparse regularization", in Optics Letters, Mar. 2014, pp. 1705-1708.

[6] F. Biscani and D. Izzo, "A parallel global multiobjective framework for optimization: pagmo", in Journal of Open Source Software, Sep. 2020, pp. 1-7.